Metals

CrossMark

High strength and ductility combination in nano-/ultrafine-grained medium-Mn steel by tuning the stability of reverted austenite involving intercritical annealing

Jun Hu[1],* (ID), Jia-Mei Zhang[1], Guo-Sheng Sun[1], Lin-Xiu Du[1], Yue Liu[1], Ying Dong[1], and R. D. K. Misra[2]

[1] *The State Key Laboratory of Rolling and Automation, Northeastern University, Shenyang 110819, China*
[2] *Laboratory for Excellence in Advanced Steel Research, Department of Metallurgical, Materials and Biomedical Engineering, University of Texas at El Paso, El Paso, TX 79968-0521, USA*

ABSTRACT

The structure–property relationship in 0.06C–5.5Mn steel subjected to different annealing temperatures and time was studied. Mn played a stronger effect on stabilizing austenite in comparison with Ni, and low-C medium-Mn steel possessed excellent hardenability. The reverse transformation of martensite to austenite occurred during intercritical annealing, and the volume fraction was first increased and then decreased on increasing annealing temperature or prolonging annealing time, indicative of change in thermal stability by element partitioning and coarsening of grain size. Correspondingly, the elongation was first increased and then decreased, consistent with the variation in the stability of reverted austenite. The yield strength was gradually decreased because of several factors, including recrystallization of α' martensite, decreased stability of reverted austenite, and coarse grain size. The maximum product of strength and ductility was obtained on annealing at 650 °C for 10 min, which was attributed to the optimal stability of reverted austenite rather than the highest volume fraction, and tensile strength and elongation were 1120 MPa and 23.3%. The strain partitioning behavior of two phases was elucidated by analyzing Lüders straining and continuous work hardening after yield point elongation, and the deformation mechanism was strongly related to the stability of reverted austenite.

Address correspondence to E-mail: hujun@ral.neu.edu.cn

Springer

Introduction

There is an increasing demand for a wide range of structural materials in consideration of cost reduction, energy saving, environmental friendly, and light weight. Strength and ductility are well recognized as the key mechanical properties of automotive steel. Strength is greatly improved via multiple strengthening mechanisms individually or in combination. Unfortunately, improving strength usually leads to the degradation of ductility; thus, great effort has been made to evade the strength–ductility trade-off dilemma [1–3].

Medium-Mn steel is defined as a steel with Mn concentration in the range of 3–10 wt%, as reported first by Miller [4]. Among the common alloying elements in steel, Mn is most attractive as a substitute for Ni considering alloy cost and similar effect on phase transformation [5]. Compared to the martensitic steel characterized by sufficient strength but unsatisfactory ductility due to lack of effective hardening and stress-releasing mechanisms, the excellent combination of strength and ductility can be obtained in medium-Mn steel through TRIP (transformation-induced plasticity) and/or TWIP (twinning-induced plasticity) effect, involving transformation of metastable austenite to martensite on the application of external stress. Martensite dominated in the hot-rolled or cold-rolled states, and the metastable austenite was obtained by reheating the steel with original martensitic microstructure in the intercritical region ($\alpha + \gamma$ two phase region) [6]. Mn diffusion and segregation to martensite lath interface plays a key role in austenite nucleation at elevated temperature, and then, austenite is stabilized by further partitioning of C and Mn from α to γ [7]. The volume fraction, morphology, dispersion, size, and element enrichment determines a broad range of mechanical properties, and can be tailored by accurately tuning alloying content and thermo-mechanical treatment. It was proposed that the prior austenite grain boundary condition and initial martensite microstructure had significant effect on structure–property relationship in medium-Mn steel and is related to transformation kinetics and microstructural characteristics. When the cold-rolled steel is intercritically annealed, recrystallization of α' martensite matrix and reverse transformation from α' martensite to γ occurred simultaneously because cold rolling introduced high dislocation density in the α' martensite matrix, resulting in a globe-shaped grain morphology [8]. Annealing procedure greatly affected the duplex microstructure and hence the mechanical properties [9, 10], whereas the effect of Mn on improving stability of austenite is still unclear in comparison with Ni. Moreover, the transformation mechanisms (nucleation and element partitioning) and deformation behavior of reverted austenite (yield behavior, Lüders strain, and work hardening) in the cold-rolled steel plate subjected to different annealing conditions require a detailed study, and the establishment of structure–property relationship is meaningful.

In the present paper, the effect of Mn and Ni on stabilizing austenite was compared via Thermo-Calc calculation. Moreover, the evolution of prior austenite grains in low-carbon medium-Mn steel under different reheating temperatures was investigated by in situ observation using high-temperature confocal laser scanning microscope. Based on the analyses of transformation behavior and deformation mechanisms of cold-rolled steel subjected to different annealing process, the relationship between structure and properties was established. The product of strength and ductility was optimized by adjusting the stability of reverted austenite.

Experimental

The experimental steel was melted in a vacuum induction furnace and cast as 155 kg ingot. The nominal chemical composition of the experimental steel in wt% was 0.06C, 0.2Si, 5.5Mn, 0.009P, 0.001S, 0.03Al, 0.4Cr, 0.2–0.7 (Cu + Ni + Mo), 0.006 N, and balance Fe. The theoretical calculations concerning evolution of FCC phase with temperature were conducted using Thermo-Calc combined with TCFE9 database (steels/Fe alloys) for comparing the effect of Ni and Mn on phase content in equilibrium. The mass percent of each element was used, and property diagram was chosen. The austenitic microstructural evolution at high temperature was in situ observed by heating to 950 °C, 1050 °C, 1150 °C, and 1200 °C for 25 min using a VL2000DX-SVF17SP&15FTC high-temperature confocal laser scanning microscope.

The schematic of rolling and annealing process of experimental steel is shown in Fig. 1. The 30-mm-thick slab was heated to 1150 °C for 3 h. After air cooling to 960 °C, followed by rolling via 5 passes on
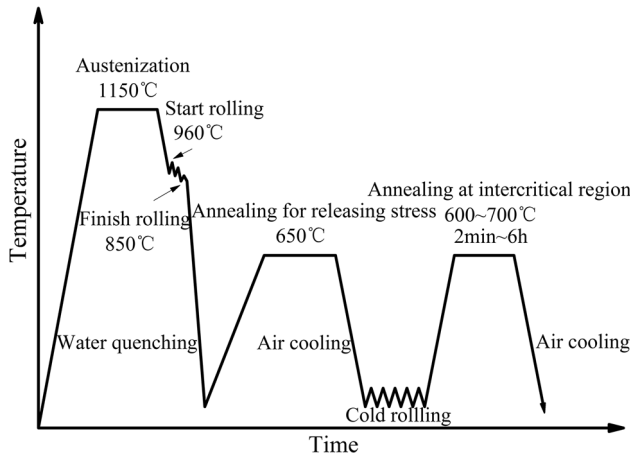
Figure 1 Schematic of rolling and annealing process of experimental steel.

a trial rolling mill with roll diameter of 450 mm, the slab was rolled to a plate of ∼ 5 mm thickness with total reduction of ∼ 83%. The finish rolling was controlled at 850 °C. Subsequently, the plate was directly water-quenched to room temperature using an accelerated cooling system. Next, for the purpose of releasing the internal stress and reducing the cold rolling force, the water-quenched plates were reheated to the annealing temperature of 650 °C for 10 min. The annealed steel plate was cold-rolled on a trial rolling mill with roll diameter of 325 mm to the thickness of ∼ 1 mm with the total reduction of ∼ 80%. Subsequently, the cold-rolled steel sheets were annealed at different temperatures of 600 °C, 630 °C, 650 °C, 670 °C, and 700 °C for 2 min, 10 min, 1 h, 4 h, and 6 h, respectively. In order to study the effect of hot rolling deformation on the refinement of quenched martensite laths, another water-quenched steel plate after hot rolling was reheated to 1150 °C for 3 h and then water-quenched to room temperature.

The specimens for microstructural studies were polished using standard metallographic procedure and etched with a 4 vol% nital solution and observed using a LEICA DMIRM optical microscope. TEM studies were conducted using 3-mm-diameter thin foils, ground to a thickness of 50 μm and electropolished using a solution of 8% perchloric acid and alcohol at − 20 °C in a twin-jet machine, and examined by FEI Tecnai G^2 F20 TEM at an accelerating voltage of 200 kV. The Mn content in austenite and ferrite was determined using energy-dispersive X-ray spectroscopy (EDX) within the TEM, and the data presented here were an average of ten measurements.

For electron backscattered diffraction (EBSD), the sample was electrolytically polished in a solution of perchloric acid and ethyl alcohol. In the orientation image map, the gray lines represent the low misorientation boundaries of 2°–15° and the black lines correspond to the high misorientation boundaries of 15° and larger than 15°. The volume fraction of austenite was determined by a D/max2400 XRD using a Co-Kα radiation source with the scanning speed of 2 deg/min, and the integrated intensities of $(200)\gamma$, $(220)\gamma$, $(311)\gamma$, $(200)\alpha$, and $(211)\alpha$ peaks were used to quantify the content of austenite using Eq. 1 [11, 12]. The specimens were mechanically ground and electropolished to minimize the possible error originating from the mechanically induced transformation of retained austenite during the specimen preparation.

$$V_\gamma = 1.4I_\gamma/(I_\alpha + 1.4I_\gamma) \tag{1}$$

where V_γ is the volume fraction of retained austenite, I_γ is the integrated intensity of the austenite peaks, and I_α is the integrated intensity of the ferrite peaks.

The tensile specimens of dimensions 1 mm thickness, 6 mm width, and 25 mm length were machined from the plates parallel to the rolling direction. The tensile tests were conducted at room temperature with a crosshead speed of 1 mm/min (corresponds to an initial strain rate of $0.67 \times 10^{-3} s^{-1}$) using a Shimadzu AG–X universal testing machine. The elongation after fracture was calculated by checking the gage length after the tensile test. The strength data are an average of three measurements.

Results and discussion

Austenite transformation behavior and thermal dynamic calculation

The optical micrographs of experimental steel after holding at different austenization temperatures are shown in Fig. 2, and the effect of reheating temperature on austenite grain size was studied, as shown in Fig. 3. When the reheating temperature was increased from 950 to 1050 °C, the austenite grain size was increased from 36.2 to 57.9 μm. Recrystallization occurred, and the equiaxed austenite grains were of near uniform size. The grain size increased to 95.9 μm on increasing the reheating temperature to 1150 °C. There were still sub-grain boundaries inside. When

Figure 2 Optical micrographs of experimental steel after holding at different austenization temperatures: **a** 950 °C; **b** 1050 °C; **c** 1150 °C; and **d** 1200 °C.
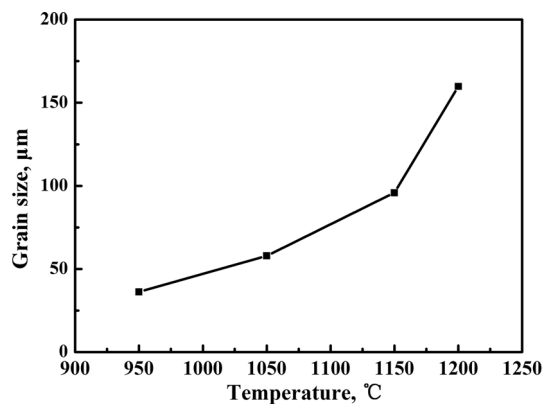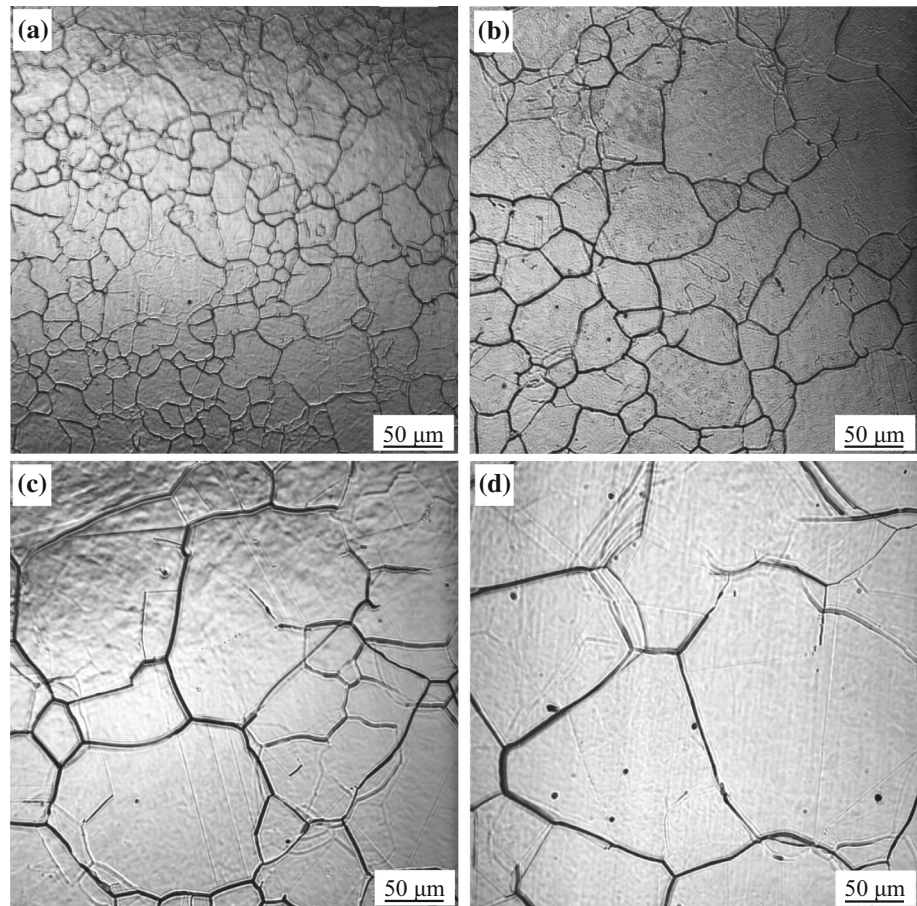

Figure 3 Effect of austenization temperature on austenitic grain size.

the reheating temperature was raised to 1200 °C, the grains were dramatically coarsened to 159.8 μm. The large density of austenitic grain boundaries in fine prior austenite grains provided considerable nucleation sites for martensitic transformation. Thus, plate and lath of martensite can be significantly refined [13]. Reheating at low temperature increases the

cohesion of austenite grains by avoiding the formation of phase with low melting point due to medium-Mn content. Therefore, the reheating temperature of thermo-mechanical-controlled process should not be greater than 1150 °C based on the condition that no microalloying precipitates are available to pin the prior austenite grain boundaries.

The effect of Ni, Mn, and C on FCC content of low-C steel was calculated using Thermo-Calc and is shown in Fig. 4. In 0.06C steel with different Ni content, Ni stabilizes the austenite and decreases the start and finish temperature of martensite to austenite transformation during heating process. Therefore, the increase in Ni content in low-C steel is beneficial in obtaining larger fraction of reverted austenite at lower annealing temperature (Fig. 4a), resulting in the refinement of microstructure. Mn plays a stronger effect in stabilizing austenite in comparison with Ni. Higher fraction of austenite existed in medium-Mn steel than medium-Ni steel, the volume fraction of austenite in 0.06C–5Mn steel at 650 °C was 38.9% in comparison with that of 23.1% in 0.06C–5Ni steel
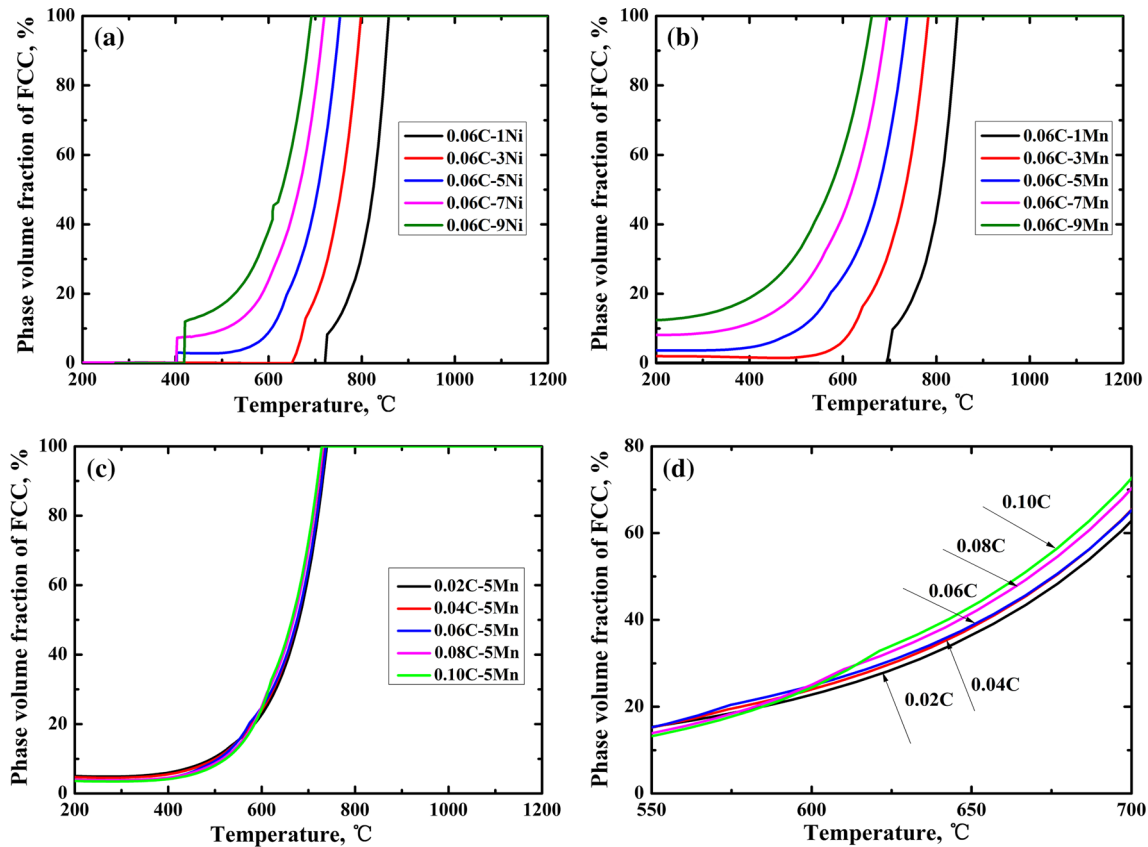
Figure 4 Effect of Ni, Mn, and C on FCC content of low-C steel calculated using Thermo-Calc: **a** steel with 0.06C and different Ni content; **b** steel with 0.06C and different Mn content; **c** steel with different C content and 5Mn; and **d** high magnification of **c**.

(Fig. 4b). Therefore, the concept of Ni substituted by Mn for obtaining metastable austenite is feasible. Moreover, there is significant merit in terms of alloy cost. The fraction of FCC phase in 5Mn steel was slightly increased by increasing the C content, whose volume fraction at 650 °C was 36.5%, 38.2%, 38.9%, 41.6%, and 43.1%, respectively, for C content of 0.02, 0.04, 0.06, 0.08, and 0.10 (Fig. 4c, d). Therefore, metastable austenite can be obtained in low-C steel with medium-Mn and/or medium-Ni addition.

The continuous cooling transformation curves of deformed austenite are shown in Fig. 5. Low-C medium-Mn steel possessed excellent hardenability. The transformation start temperature of martensite was in the range of ∼ 370–390 °C at cooling rate of 0.1–60 °C/s. Therefore, fine martensite plate was likely to be obtained during the cooling process followed by hot rolling, and multiple cooling conditions including water quenching, accelerated cooling, and air cooling were feasible.
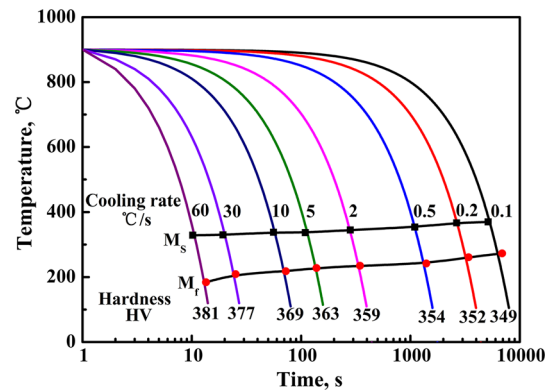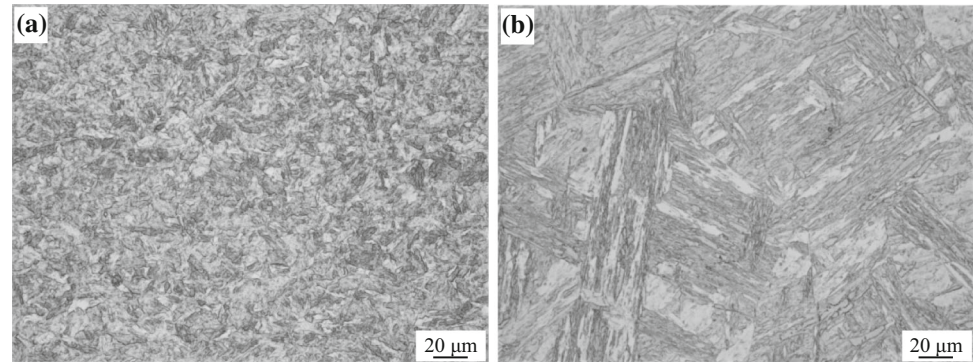

Figure 5 Continuous cooling transformation curves of deformed austenite.

Effect of annealing temperature and time on microstructural evolution

Optical micrographs of hot-rolled experimental steels are shown in Fig. 6. Fine martensite laths were formed inside small prior austenite grains in the hot-rolled steel subjected to direct quenching (Fig. 6a).

On the contrary, coarse martensite plates were obtained within large prior austenite grains when the plate was reheated to 1150 °C for 3 h and subsequently quenched to room temperature (Fig. 6b). Thus, hot rolling dramatically refined the prior austenite grains and provided an amount of nucleation sites for martensite transformation, such that the microstructure refinement was conducive to increase the overall homogenization of material. The blocky austenite with lower stability nucleated at coarse prior grain boundaries, and cleavage crack initiated when stress-induced coarse blocky austenite transformed to martensite prematurely [14, 15]. Moreover, coarse prior austenite grain boundaries decorated by C, Mn, and P encouraged the formation of intergranular cracking, and hot-rolled deformation promoted the elimination of solute-decorated boundaries of coarse prior γ grains because increased austenite grain boundaries by recrystallization diluted these decorated solutes [16]. As a result, the cohesion of austenite boundaries was increased.
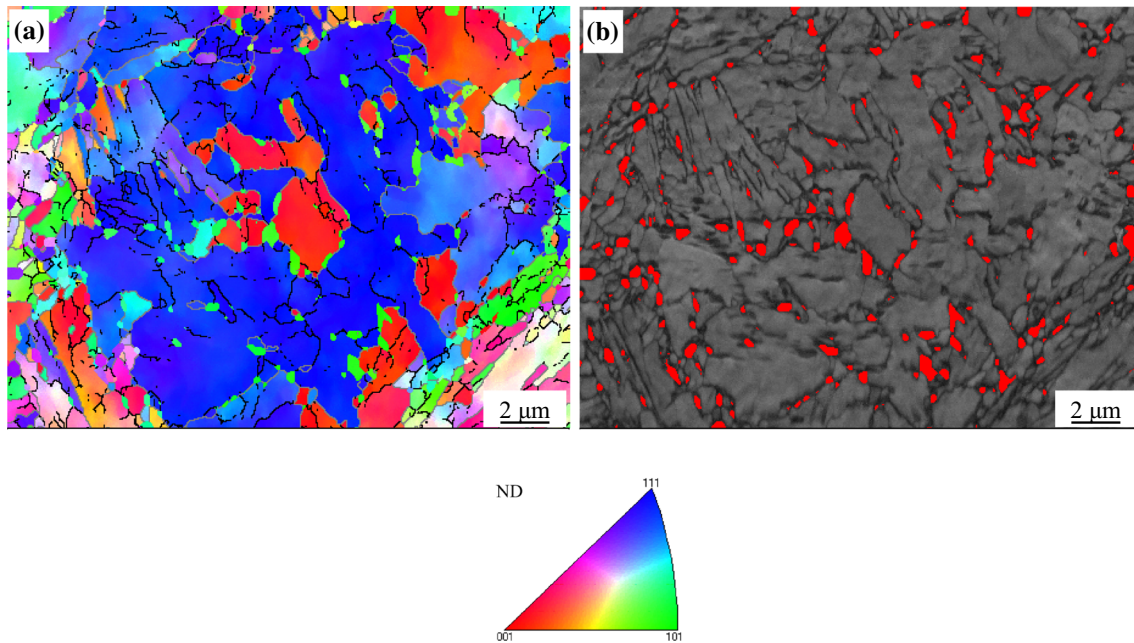
TEM micrographs of directly quenched experimental steel subjected to annealing at 650 °C for 10 min are shown in Fig. 7, and the crystallographic characteristics analyzed by EBSD are shown in Fig. 8. The quenched martensite laths were recovered during the annealing process accompanied by rejection of C atoms from the interior of martensitic laths to the lath interface and annihilation of dislocations at the same time. The literatures proposed that the strong interface segregation of austenite stabilizing elements C and Mn, and the release of stress from host martensite stimulated austenitic reversion transformation at lath boundaries [17, 18]. The reverted austenite of block shape was predominately formed along the prior austenite grain boundaries, and also, a small amount austenite nucleated at the martensitic packets boundaries.

TEM micrograph of cold-rolled experimental steel is shown in Fig. 9. Cold rolling after alloy partitioning destroyed the orientation relationship between ferrite and austenite and also decreased the interlayer spacing [19], and the metastable austenite was transformed to lath martensite subjected to continuous cold rolling. The substructure of sub-grains, dislocations, and voids formed inside the martensite
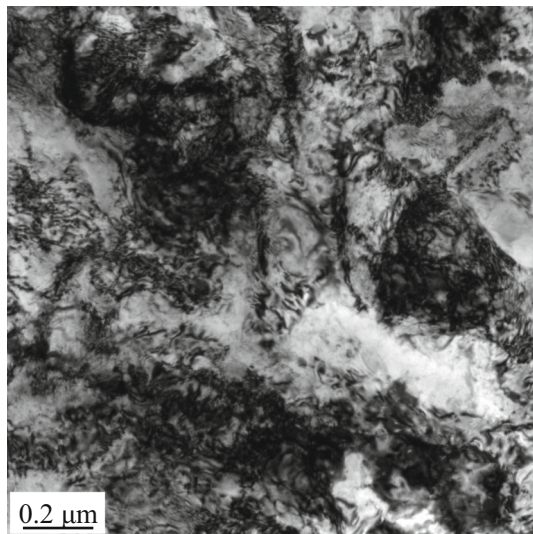
Figure 7 TEM micrographs of experimental steel subjected to hot rolling, directly quenching, and annealing at 650 °C for 10 min: **a** bright-field image of low magnification; **b** dark-field image of high magnification.
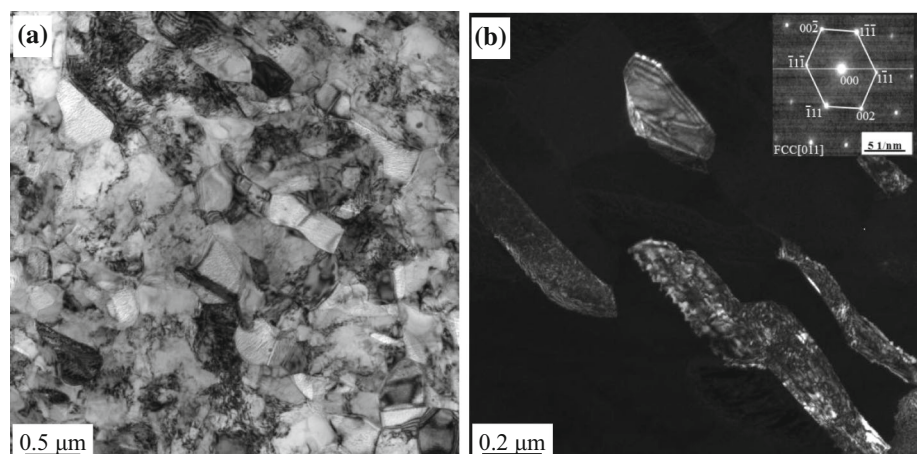
Figure 8 Crystallographic characteristics of experimental steel subjected to hot rolling, directly quenching, and annealing at 650 °C for 10 min analyzed by EBSD: a orientation image map with grain boundary misorientation distribution; **b** image quality map with reverted austenite in red.
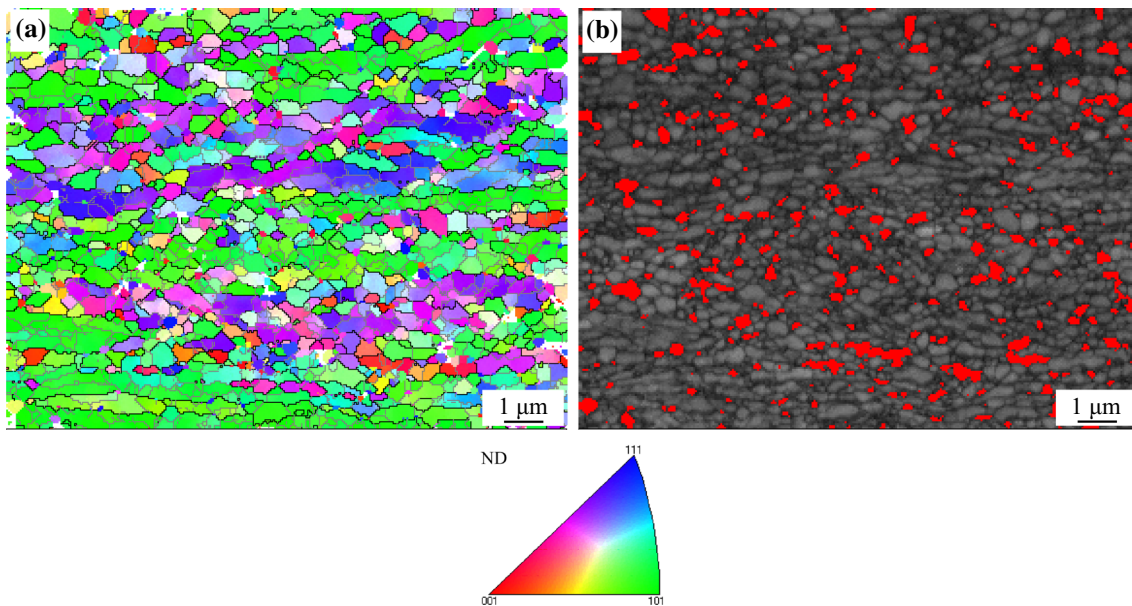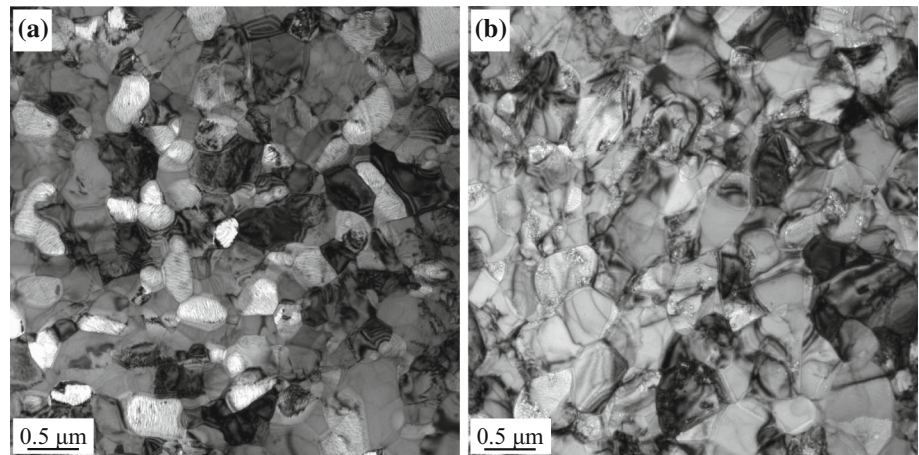

Figure 9 TEM micrograph of cold-rolled experimental steel.

laths during further cold rolling deformation. It was proposed that cold rolling deformation actively encourages Mn partitioning, and is probably attributed to the accelerated diffusion of Mn, which is assisted by crystal defects such as dislocations, elongated grain boundaries, and vacancies [20]. The TRIP effect exerted by the transformation of metastable austenite to martensite was beneficial in

reducing the cold rolling force, and cracking was avoided because of release of stress.

The TEM micrographs of cold-rolled experimental steels subjected to annealing at 650 °C for different time are shown in Fig. 10, and the crystallographic characteristics of cold-rolled experimental steel subjected to annealing at 650 °C for 10 min analyzed by EBSD are shown in Fig. 11. The deformed martensite laths with high density of defects, including sub-grain boundaries and dislocations, were recrystallized at elevated temperature, and the reverse transformation from martensite to austenite occurred simultaneously. The formation of globe-shaped reverted austenite grains indicated the reversion mechanism was diffusive rather than displacive [21]. The austenite grains were gradually increased with prolonged annealing time, and the average size was 80 nm, 210 nm, 380 nm, 620 nm, and 800 nm, respectively, for annealing time of 2 min, 10 min, 1 h, 4 h, and 6 h. The crystallographic characteristics of prior austenite grains were completely destroyed by heavy cold rolling deformation. The annealed steel demonstrated uniform distribution of orientation along the deformation band. The reverted austenite of granular shape was dispersedly nucleated at the cold-rolled martensite matrix.

Figure 10 TEM micrographs of cold-rolled experimental steels subjected to annealing at 650 °C for different time: **a** 10 min; **b** 1 h.


Figure 11 Crystallographic characteristics of cold-rolled experimental steel subjected to annealing at 650 °C for 10 min analyzed by EBSD: **a** orientation image map with grain boundary misorientation distribution; **b** image quality map with reverted austenite in red.

The relationship between annealing at 650 °C for different time and the volume fraction of reverted austenite is shown in Fig. 12. The partitioning of Mn atoms occurred from the internal of martensite lath to

Figure 12 Relationship between annealing at 650 °C for different time and the volume fraction of reverted austenite: **a** XRD spectra; **b** volume fraction of reverted austenite.
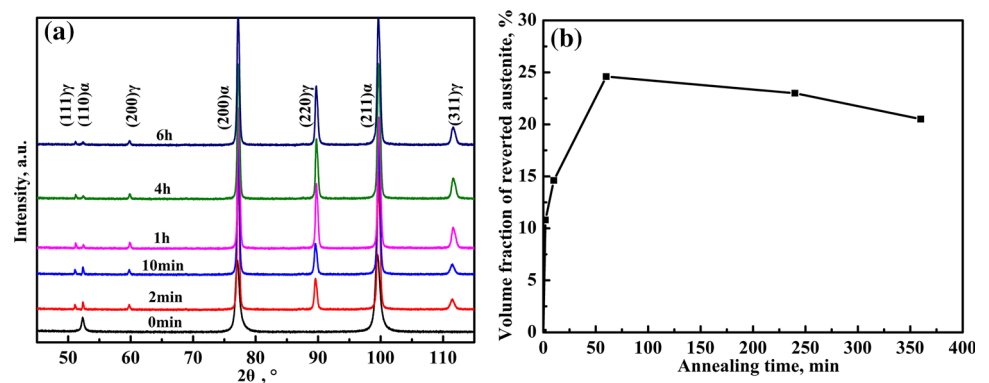
the interface during the annealing process. When annealing was conducted at 650 °C for 10 min, the Mn content in austenite grains and the adjacent equiaxed ferrite grains was 8.30 and 2.19 in wt%, respectively. On increasing the annealing time from 10 min to 1 h, the content of Mn decreased to 7.68 in wt%. The volume fraction of reverted austenite was significantly increased on prolonging the annealing time from 2 min to 1 h. Subsequently, the amount was slightly reduced with the increase in annealing time. The volume fraction of austenite was 10.8%, 14.6%, 24.6%, 23.0%, and 20.5% respectively, at annealing time of 2 min, 10 min, 1 h, 4 h, and 6 h. The reduction of reverted austenite was attributed to the decrease in thermal stability due to weak enrichment of element and coarse grain size [22], such that the less stable austenite was transformed to second martensite during cooling.

TEM micrographs of experimental steels subjected to annealing at different temperatures for 10 min are shown in Fig. 13. The grain size of austenite was increased with the increase in annealing temperature, which was 180 nm, 210 nm, 460 nm, and 780 nm, respectively, at annealing temperature of 630 °C, 650 °C, 670 °C, and 700 °C. The reverse transformation rate was greatly increased with annealing temperature because of the increase in atomic diffusion of C and Mn with the increase in temperature. The content of Mn was correspondingly decreased with the increase in annealing temperature, which was 8.30, 7.78, and 5.99 in wt%, respectively, at annealing temperature of 650 °C, 670 °C, and 700 °C.
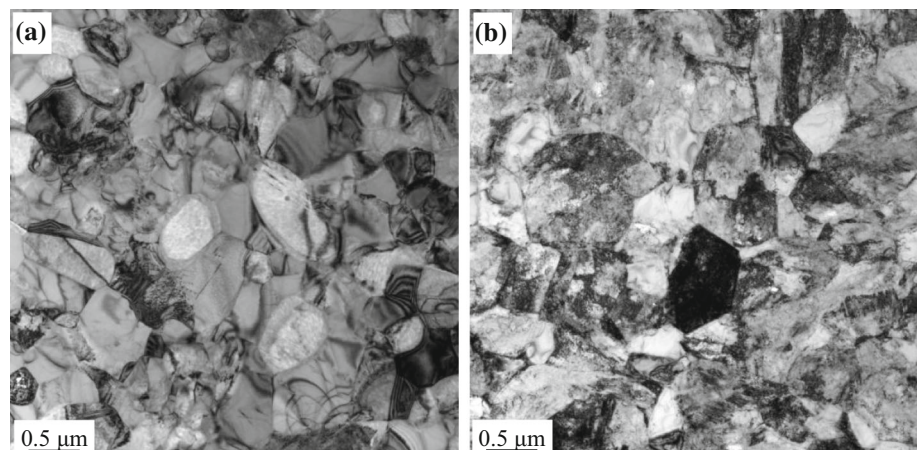
Relationship between annealing temperature and volume fraction of reverted austenite analyzed by XRD is shown in Fig. 14. The volume fraction of reverted austenite was gradually increased with increased annealing temperature from 600 to 670 °C and then drastically decreased with further increase in annealing temperature to 700 °C. The volume fraction of reverted austenite was 6.8%, 13.9%, 14.6%, 19.2%, and 3.4%, respectively, at annealing temperature of 600 °C, 630 °C, 650 °C, 670 °C, and 700 °C. Based on the calculation using Thermo-Calc, the content of austenite should increase with annealing temperature, while the content was sharply decreased when the temperature was higher than 670 °C. The size of reverted austenite was dramatically increased, and the enrichment of Mn inside austenite was correspondingly reduced. As a result, the thermal stability was reduced, and reverted austenite was transformed to martensite during subsequent cooling process. During the annealing process, Mn and C atoms were supersaturated in quenched martensite laths, such that Mn diffused from the interior of martensitic lath to the lath boundaries, whereas the cohesion of lath boundaries was deteriorated during early stage of reverse transformation due to the harmful effect of Mn segregation [23]. With progress in diffusion, the interface cohesion was improved because of the decrease in Mn segregation by continuous partitioning into the newly formed γ.

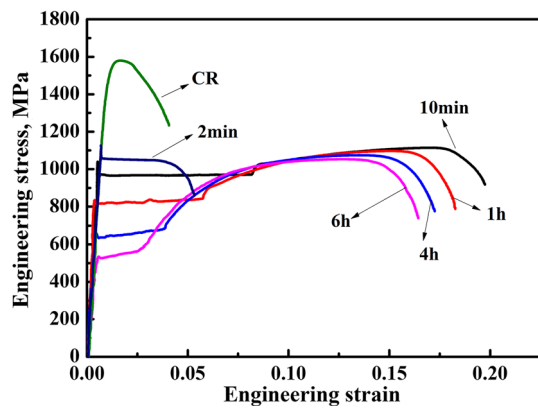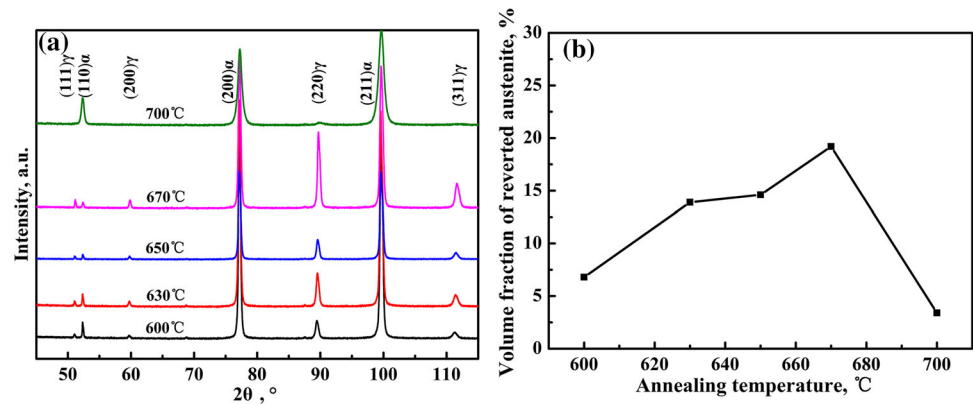## Effect of annealing temperature and time on mechanical properties

Engineering stress–strain curves of experimental steel annealed at 650 °C for different time are shown in Fig. 15, and the relationship between annealing time and mechanical properties of experimental steel is

Figure 13 TEM micrographs of experimental steels subjected to annealing at different temperatures for 10 min: **a** 670 °C; **b** 700 °C.
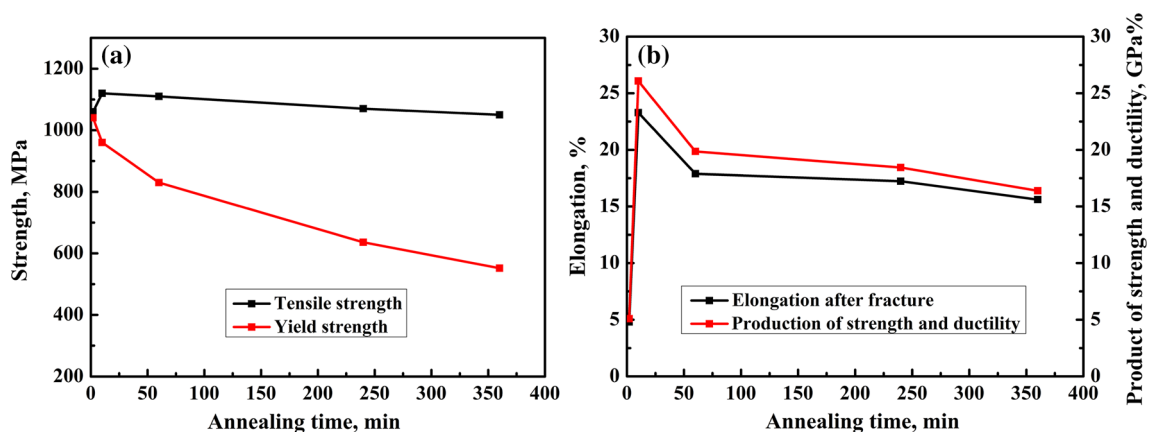
Figure 14 Relationship between annealing temperature and volume fraction of reverted austenite analyzed by XRD: **a** XRD spectra; **b** volume fraction of reverted austenite.

Figure 15 Engineering stress–strain curves of experimental steel annealed at 650 °C for different time.


and 552 MPa, respectively, at annealing time of 2 min, 10 min, 1 h, 4 h, and 6 h, and attributed to several factors, including recovery and recrystallization of cold-rolled hardened martensite laths, reduced density of dislocations and substructure, increased content and decreased stability of reverted austenite, and coarse grain size. The decrease in tensile strength was much less in comparison with yield strength due to the significant role of enhanced work hardening played from metastable austenite. The elongation was first increased from 4.80 to 23.28% on prolonging the annealing time from 2 to 10 min and then decreased to 17.89%, 17.23%, and 15.61% when the annealing time was 1 h, 4 h, and 6 h. The maximum product of strength and ductility was obtained at the annealing time of 10 min. When the annealing time was 2 min, the content of reverted austenite was inadequate. Moreover, the mechanical stability of fine reverted austenite was excessively high, such that the elongation was low due to inadequate TRIP effect. A yield plateau emerged. When

shown in Fig. 16. The cold-rolled steel possessed high yield strength of 1450 MPa and tensile strength of 1580 MPa, but the elongation was extremely low at 4.2% due to lack of work hardening ability. On increasing the annealing time, the yield strength was gradually decreased, which was 1040, 960, 830, 636,

Figure 16 Relationship between annealing time and mechanical properties of experimental steel: **a** strength as a function of annealing time; **b** elongation and product of strength and ductility as a function of annealing time.

the annealing time was increased to 10 min, the content of austenite was increased. Moreover, the element enrichment inside reverted austenite was weaker because of continuous progress in partition, and the size of reverted austenite was coarsened. As a consequence, the mechanical stability of reverted austenite was adjusted to be appropriate for exerting the optimal TRIP effect. The elongation was dramatically improved by the enhanced work hardening ability, associated with metastable austenite under tensile strain. There was significant yield point elongation regime, where both ferrite and austenite phase deformed plastically by glide. When the annealing time was further increased to 1 h, the decreased stability of reverted austenite was transformed to earlier strain, leading to the slightly reduced elongation. The Lüders bands were gradually shortened with the increase in annealing time.
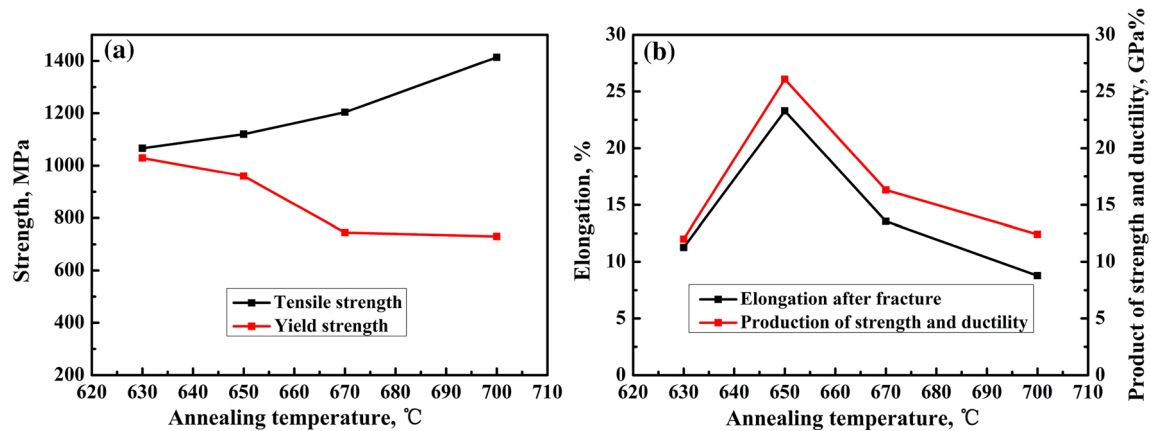
Engineering stress–strain curves of experimental steel annealed at different temperatures for 10 min are shown in Fig. 17, and relationship between annealing temperature and mechanical properties of experimental steel is shown in Fig. 18. As the annealing temperature was increased, the yield strength was decreased from 1029, 960, 745 to 730 MPa, at annealing temperature of 630, 650, 670, and 700 °C, and the tensile strength was significantly increased from 1066, 1120, 1204 to 1414 MPa due to increased strain hardening rate caused by the enhanced TRIP effect. The elongation was first increased from 11.26 to 23.28% with the increase in annealing temperature from 630 to 650 °C and then decreased sharply to 13.55% and 8.78% at 670 °C and 700 °C. The product of strength and ductility was
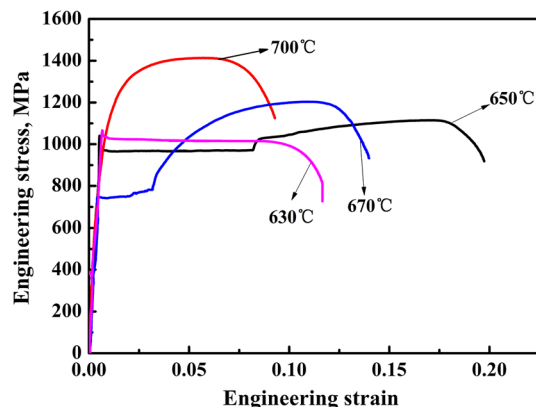
greatly affected by elongation with highest point obtained at 650 °C. When annealing was conducted at 630 °C, the elongation was improved in comparison with cold-rolled condition, and the Lüders bands were formed. As the annealing temperature was increased to 650 °C, the elongation was remarkably enhanced. Moreover, there was very strong and continuous work hardening behavior during further straining after yield point elongation regime. These reverted austenite grains have a wide range of mechanical stability, such that the TRIP effect was enhanced by the sustainable transformation from austenite to martensite during deformation rather than in a very short period. This contributed to a more thorough load distribution between fine recrystallized ferrite grains and reverted austenite [6]. Dislocation glide in martensite and ferrite dominated the initial deformation stage; with the increase in strain, the reverted austenite transformed to martensite, and constrained ferrite relaxed with volume expansion associated with martensite transformation. The transformed martensite strengthened the local region and suppressed nucleation and growth of microvoids and/or microcracks [24]. On annealing at 670 °C, the yield strength was significantly decreased, and the tensile strength was enhanced. The elongation was deteriorated, and the Lüders bands were greatly shortened. When the annealing temperature was further increased to 700 °C, Lüders bands completely disappeared, yielding was continuous and the deformation remained homogeneous on further straining. The tensile stress–strain behavior was similar to two phase steel. In comparison with annealing time, annealing temperature played more significant role on thermal stability and mechanical stability of reverted austenite.

The stress–strain behavior of cold-rolled and annealed medium-Mn steel was dominated by the dynamic stain partitioning of recrystallized ferrite and reverted austenite, and significantly affected by the annealing procedure. When annealing was conducted at low temperature for short duration, yielding was initiated on plastic deformation of recrystallized ferrite due to low dislocation density involving active recovery and lower concentration of Mn and C. Moreover, the reverted austenite was difficult to be deformed because of the solid solution hardening of Mn and C [8], and the yielding was proceeded by Lüders band nucleation and propagation at constant stress. The literature suggests that in

Figure 17 Engineering stress–strain curves of experimental steel annealed at different temperatures for 10 min.

Figure 18 Relationship between annealing temperature and mechanical properties of experimental steel: **a** strength as a function of annealing temperature; **b** elongation and product of strength and ductility as a function of annealing temperature.

the yield point elongation range, the austenite deforms by glide of partial dislocations trailing stacking faults. The Lüders plateau is related to the localization of the strain in the absence of work hardening, whereas such pronounced localization did not lead to sudden fracture in spite of submicron-scale grain size [10, 25]. In low-carbon ferritic steel, Lüders strain was larger in fine-grained steel in comparison with coarse-grained steel because grain boundaries act as obstacles to the movement of Lüders bands and reduce their propagation velocity [26].

A higher annealing temperature for longer duration resulted in larger fraction of reverted austenite with coarser grain size and lower chemical stability. The reverted austenite underwent martensite transformation during post-annealing cooling, resulting in less volume fraction of austenite and a higher dislocation density in the ferrite. This provided sufficient mobility to dislocations so as to suppress static strain aging and led to reduction in the ferrite yield stress. Yielding was triggered by active stress-induced transformation of retained austenite islands with reduced stability, contributing to suppression of localization of plastic flow [10].

Conclusions

1. Based on the calculation using Thermo-Calc, Mn played a stronger effect on stabilizing austenite in comparison with Ni. Higher fraction of austenite existed in medium-Mn steel than medium-Ni steel. Low-C medium-Mn steel possessed

excellent hardenability. The transformation start temperature of martensite was in the range of ∼ 370–390 °C at cooling rate of 0.1–60 °C/s.

2. The grain size of prior austenite was significantly increased from 95.9 μm to 159.8 μm when the reheating temperature was increased from 1150 °C to 1200 °C. The reheating temperature of thermo-mechanical-controlled process should not be greater than 1150 °C from the viewpoint of increasing grain boundaries cohesion and refinement of martensite laths.

3. Hot rolling deformation dramatically refined prior austenite grains, resulting in significant refinement of quenched martensite lath. The reverse transformation of martensite to austenite occurred during intercritical annealing, and the volume fraction of reverted austenite was significantly increased on prolonging the annealing time from 2 min to 1 h, subsequently reducing. The volume fraction of reverted austenite was gradually increased on increasing the annealing temperature from 600 to 670 °C and then drastically decreased on further increasing the annealing temperature to 700 °C. The reduction of reverted austenite at high annealing temperature or long annealing time is attributed to the decrease in thermal stability due to weak element enrichment and coarse grain size.

4. With the increase in annealing temperature or prolonging annealing time in the intercritical zone, the yield strength was gradually decreased due to several factors, including recovery and recrystallization of cold-rolled hardened martensite laths, reduced density of dislocations and

substructure, increased content and decreased stability of reverted austenite, and coarse grain size. The elongation was first increased and then decreased, attributed to the stability of reverted austenite. The maximum product of strength and ductility was obtained at annealing temperature of 650 °C for 10 min.

5. Lüders band formed after intercritical annealing at low temperature for short time, but did not lead to the reduction in elongation in spite of submicron-scale grain size. There was very strong and continuous work hardening behavior during further straining after yield point elongation regime, indicated sustainable TRIP effect played by reverted austenite grains with a wide range of mechanical stability. The Lüders bands were shortened and finally disappeared with further increase in the annealing temperature because of the decreased stability of reverted austenite and formation of second martensite.

Acknowledgements

Compliance with ethical standards

Conflict of interest The authors declare that they have no conflict of interest.

References

[1] He BB, Hu B, Yen HW, Cheng GJ, Wang ZK, Luo HW, Huang MX (2017) High dislocation density-induced large ductility in deformed and partitioned steels. Science 357:1029–1032

[2] Kim SH, Kim H, Kim NJ (2015) Brittle intermetallic compound makes ultra-strong low-density steel with large ductility. Nature 518:77–79

[3] Wei YJ, Li YQ, Zhu LC, Liu Y, Lei XQ, Wang G, Wu YX, Mi ZL, Liu JB, Wang HT, Gao HJ (2014) Evading the strength-ductility trade-off dilemma in steel through gradient hierarchical nanotwins. Nat Commun 5:1–8

[4] Miller RL (1972) Ultrafine-grained microstructures and mechanical properties of alloy steels. Metall Trans A 3:905–912

[5] Nikura M, Morris JW (1980) Thermal processing of ferritic 5Mn steel for toughness at cryogenic temperatures. Metall Trans A 11A:1531–1540

[6] Hu B, Luo HW, Yang F, Dong H (2017) Recent process in medium-Mn steels made with new designing strategies, a review. J Mater Sci Technol 33:1457–1464

[7] Kuzmina M, Ponge D, Raaba D (2015) Grain boundary segregation engineering and austenite reversion turn embrittlement into toughness: example of a 9 wt% medium Mn steel. Acta Mater 86:182–192

[8] Han J, Lee SJ, Jung JG, Lee YK (2014) The effects of the initial martensite microstructure on the microstructure and tensile properties of intercritically annealed Fe–9Mn–0.05C steel. Acta Mater 78:369–377

[9] Luo HW, Shi J, Wang C, Cao WQ, Sun XJ, Dong H (2011) Experimental and numerical analysis on formation of stable austenite during the intercritical annealing of 5Mn steel. Acta Mater 59:4002–4014

[10] Cooman BCD, Gibbs P, Lee S, Matlock DK (2013) Transmission electron microscopy analysis of yielding in ultrafine-grained medium Mn transformation-induced plasticity steel. Metall Mater Trans A 44A:2563–2572

[11] Li Z, Wu D (2006) Effects of hot deformation and subsequent austempering on the mechanical properties of Si–Mn TRIP steels. ISIJ Int 46:121–128

[12] Xie ZJ, Han G, Zhou WH, Zeng CY, Shang CJ (2016) Study of retained austenite and nano-scale precipitation and their effects on properties of a low alloyed multi-phase steel by the two-step intercritical treatment. Mater Charact 113:60–66

[13] Sista V, Nash P, Sahay SS (2007) Accelerated bainitic transformation during cyclic austempering. J Mater Sci 42:9112–9115. https://doi.org/10.1007/s10853-007-2065-0

[14] Ding R, Tang D, Zhao A (2014) A novel design to enhance the amount of retained austenite and mechanical properties in low-alloyed steel. Scr Mater 88:21–24

[15] Hu J, Du LX, Xu W, Zhai JH, Dong Y, Liu YJ, Misra RDK (2018) Ensuring combination of strength, ductility and toughness in medium-manganese steel through optimization of nano-scale metastable austenite. Mater Charact 136:20–28

[16] Han J, Silva AKD, Ponge D, Raabe D, Lee SM, Lee YK, Lee SI, Wang BH (2017) The effect of prior austenite grain boundaries and microstructural morphology on the impact toughness of intercritically annealed medium Mn steel. Acta Mater 122:199–206

[17] Raabe D, Sandlöbes S, Millán J, Ponge D, Assadi H, Herbig M, Choi PP (2013) Segregation engineering enables nanoscale martensite to austenite phase transformation at grain boundaries: a pathway to ductile martensite. Acta Mater 61:6132–6152

[18] Raabe D, Herbig M, Sandlöbes S, Li Y, Tytko D, Kuzmina M, Ponge D, Choi PP (2014) Grain boundary segregation engineering in metallic alloys: a pathway to the design of interfaces. Curr Opin Solid State Mater 18:253–261

[19] Heo YU, Suh DW, Lee HC (2014) Fabrication of an ultra-fine-grained structure by a compositional pinning technique. Acta Mater 77:236–247

[20] Lee YK, Han J (2015) Current opinion in medium manganese steel. Mater Sci Technol lond 31:843–856

[21] Han J, Lee YK (2014) The effects of the heating rate on the reverse transformation mechanism and the phase stability of reverted austenite in medium Mn steels. Acta Mater 67:354–361

[22] Yang HS, Bhadeshia HKDH (2009) Austenite grain size and martensite-start temperature. Scr Mater 60:493–495

[23] Heo NH, Nam JW, Heo YU, Kim SJ (2013) Grain boundary embrittlement by Mn and eutectoid reaction in binary Fe–12Mn steel. Acta Mater 61:4022–4034

[24] Liu S, Xiong Z, Guo H, Shang C, Misra RDK (2017) The significance of multi-step partitioning: processing–structure–property relationship in governing high strength-high ductility combination in medium-manganese steels. Acta Mater 124:159–172

[25] Lee S, Lee SJ, Kumar SS, Lee K, Cooman BCD (2011) Localized deformation in multiphase, ultra-fine-grained 6pct Mn transformation-induced plasticity steel. Metall Mater Trans A 42A:3638–3651

[26] Hu H (1983) Effect of solutes on lüders strain in low-carbon sheet steels. Metall Trans A 14A:85–91